JOURNAL OF GEOPHYSICAL RESEARCH, VOL. 113, B08210, doi:10.1029/2007JB005466, 2008

Lava dome growth and mass wasting measured by a time series of ground-based radar and seismicity observations

G. Wadge,[1] D. G. Macfarlane,[2] H. M. Odbert,[1] M. R. James,[3] J. K. Hole,[1] G. Ryan,[4,5] V. Bass,[4] S. De Angelis,[4,5] H. Pinkerton,[3] D. A. Robertson,[2] and S. C. Loughlin[4,5]

Received 25 October 2007; revised 20 March 2008; accepted 7 May 2008; published 28 August 2008.

[1] Exogenous growth of Peléean lava domes involves the addition of lava from a central summit vent and mass wasting on the flanks as rockfalls and pyroclastic flows. These processes were investigated at the Soufrière Hills Volcano, Montserrat, between 30 March and 10 April 2006, using a ground-based imaging millimeter-wave radar, AVTIS, to measure the shape of the dome and talus surface and rockfall seismicity combined with camera observations to infer pyroclastic flow deposit volumes. The topographic evolution of the lava dome was recorded in a time series of radar range and intensity measurements from a distance of 6 km, recording a southeastward shift in the locus of talus deposition with time, and an average height increase for the talus surface of about 2 m a day. The AVTIS measurements show an acceleration in lava extrusion rate on 5 April, with a 2-day lag in the equivalent change in the rockfall seismicity record. The dense rock equivalent volumetric budget of lava added and dispersed, including the respective proportions of the total for each component, was calculated using: (1) AVTIS range and intensity measurements of the change in summit lava ($\sim 1.5 \times 10^6$ m^3, 22%), (2) AVTIS range measurements to measure the talus growth ($\sim 3.9 \times 10^6$ m^3, 57%), and (3) rockfall seismicity to measure the pyroclastic flow deposit volumes ($\sim 1.4 \times 10^6$ m^3, 21%), which gives an overall dense rock equivalent extrusion rate of about 7 m$^3 \cdot$s^{-1}. These figures demonstrate how efficient nonexplosive lava dome growth can be in generating large volumes of primary clastic deposits, a process that, by reducing the proportion of erupted lava stored in the summit region, will reduce the likelihood of large hazardous pyroclastic flows.

Citation: Wadge, G., et al. (2008), Lava dome growth and mass wasting measured by a time series of ground-based radar and seismicity observations, *J. Geophys. Res.*, *113*, B08210, doi:10.1029/2007JB005466.

1. Introduction

[2] Lava domes are large rock masses that form complex, changing shapes as they grow. They are intrinsically unstable, producing talus slopes from rockfall mass wasting and generating pyroclastic flows from larger episodes of gravitational collapse that expose pressurized lava to the atmosphere. Such collapses tend to occur where new lava is added to the surface, a process that is important from the perspective of hazard evaluation [*Calder et al.*, 2002]. The rate at which the dome grows is of similar significance, because a hotter, more pressurized interior, which may result from a high effusion rate, can be more liable to explosive disintegration. Consequently, the measurement of shape, locus of growth and lava extrusion rate are all of critical importance to understanding the process of lava dome growth and, in order to calculate the total extrusion rate, simultaneous measurements of all the mass wasting deposits must also be carried out.

[3] However, such comprehensive measurements are seldom possible due to lack of close access, the dome being obscured by cloud, and pyroclastic flow deposits (often located in valley bottoms) being unobservable from many remote viewing locations. Opportunistic measurements using optical instruments (e.g., lidar surveys [*Jones*, 2006]) are generally too infrequent, due to cloud cover, to capture dome growth dynamics. In this paper we describe the deployment of a portable ground-based radar instrument (AVTIS, All-weather Volcano Topographic Imaging Sensor), to make a continuous time series of topographic measurements of the growing dome at Soufrière Hills, Montserrat. To account for mass wasting from the dome, the results are combined with simultaneous assessments of rockfall and pyroclastic deposit volumes made from seismic and photographic data. This has allowed the total extrusion rate to be estimated, and has also provided the relative proportions by

[1] Environmental Systems Science Centre, University of Reading, Reading, UK.
[2] School of Physics and Astronomy, University of St. Andrews, St. Andrews, UK.
[3] Lancaster Environment Centre, Lancaster University, Lancaster, UK.
[4] Montserrat Volcano Observatory, Flemmings, Montserrat, West Indies.
[5] British Geological Survey, Edinburgh, UK.

0148-0227/08/2007JB005466$09.00

Table 1. AVTIS Technical Characteristics

Parameter	Value
Frequency	94 GHz
Radar range resolution	0.85 m
Radiometric thermal sensitivity	<5 K
Antenna size	300 mm
Two-way radar beam width	0.5°
Radiometric beam width	0.7°
Radar transverse resolution (per km)	8.7 m
Radar signal-to-noise at long range	−0.35 dB at 6 km
Data sampling rate	500 kHz
Maximum pixel integration time	32 ms
Image acquisition time (10° × 5°, 0.1° inc.)	20 min
Power consumption	115 W
Continuous operational duration	8 h

which the extruded lava was being partitioned into talus, pyroclastic flow deposits and lava dome "core."

[4] AVTIS is a millimeter-wave dual-mode radar/radiometer (radarometer) instrument [*Macfarlane and Robertson*, 2004] that can image topography and map surface temperature variations, through clear air or cloud (its technical capabilities are summarized in Table 1). Thus, at frequently cloud-covered volcanoes such as Soufrière Hills, the instrument is capable of obtaining a time series of topographic measurements with a frequency and continuity not possible by other techniques. AVTIS has been used previously at Montserrat to record topography and to estimate the extrusion rate and temperature of the dome lava [*Wadge et al.*, 2005, 2006], and to measure lava flow advance at Arenal, Costa Rica [*Macfarlane et al.*, 2006]. The data set described here, collected over two weeks in March to April 2006, represents the first dense time series of a growing lava dome.

[5] The current eruption of Soufrière Hills Volcano began in 1995, and has produced a series of Peléean lava domes of andesitic composition within a crater (English's Crater) open to the east northeast [*Watts et al.*, 2002] (Figure 1). These domes, fed from a central conduit within the crater, have been destroyed by collapse and explosion, usually producing pyroclastic flows, and have regrown repeatedly during three episodes of lava extrusion (1995–1998; 1999–2003; 2005–2007). Six weeks after the field campaign reported here, the lava dome was destroyed on 20 May 2006, with most of the material being deposited in the sea to the east. At times during the ongoing twelve-year eruption, the dome at Soufrière Hills has grown up to 1000 m in diameter and up to 400–450 m in height. The elevation of the crater floor at the conduit vent is about 700 m above sea level (asl) and the rim of the crater is at about 800 m asl. The elevations of both the crater floor and the northeastern crater rim fall toward the sea to the east northeast. As the dome grows within the crater, any pyroclastic flows and rockfalls are constrained by the crater walls until the summit of the dome reaches an elevation of about 950 m asl [*Wadge*, 2008]. Above this, talus can spill out over the crater rim. At the time of the observations reported here the summit of the dome was at an elevation of 900–950 m asl and the talus was still contained within the crater (Figure 2).

[6] During the early stages of development, a dome typically grows as a contiguous flowing mass. Such endogenous growth is later replaced by exogenous additions of lava at the surface via shear-bounded surfaces through the earlier lava mass (Figure 2). This mechanism allows the locus of extrusion to switch from one side of the dome to another [*Watts et al.*, 2002]. Surrounding the lava core of the dome is an apron of talus at an angle of repose of about 37°, derived from disintegration of blocks of lava from the top of the dome. This talus forms an increasingly large proportion of the whole dome as it grows. There are two main surficial processes that result in morphological change of the exogenous lava dome: addition of lava as contiguous masses or large (~10 m) blocks at the top of the dome, and the fragmentation of this lava to produce talus by rockfall and pyroclastic flow deposits.

[7] Rockfalls, and the avalanches they generate, are rapid movements of rock mass under gravity, and originate on steep slopes. The dimensions of the rockfall at source are largely defined by the jointing in the rock mass, and the failure of a large mass (longest dimension >10 m) may be followed by disintegration along its joint planes. Individual rocks may bounce, slide or roll down the slope. They may also collide with each other and these events, if numerous enough, can generate a granular mass in a state of mechanical fluidization. Experiments show that rocks at the front of such a mass accelerate forward as a result of this process, and rocks at the rear decelerate [*Okura et al.*, 2000]. This results in a greater areal coverage of deposit than would be the case if the rocks fell individually. In addition, rock clasts may also fragment under shear stress, particularly at pressure and depth in the flow [*Davies et al.*, 1999]. This fragmentation process will itself create an additional dispersive stress that, like the mechanical fluidization process, will tend to cause the avalanche mass to inflate and spread.

[8] Rockfall from active lava bodies, as at Soufrière Hills, has the additional factor of vesicular gas within the rock. This pressurized gas can lead to a sort of rapid exfoliation of the hot lava surface, producing ash [*Calder et al.*, 2002], a process also observed at other lava domes such as Unzen [*Sato et al.*, 1992]. *Calder et al.* [2002] distinguished between "passively generated" rockfalls derived from the cold carapace of the dome that are deposited to form the talus, and "actively generated" rockfalls derived from freshly extruded lava fronts. The former were seen as being largely degassed, with runouts rarely extending beyond 500 m from the source and with an upper volume of about 10^3 m^3, the latter as being gas-rich and grading into small pyroclastic flows. Auto-fragmentation is therefore probably the dominant process in both the generation and mobility of pyroclastic density currents derived from lava dome collapse and also in the long runout character of large rockfall avalanches [*Davies et al.*, 1999].

[9] The AVTIS data enabled estimates to be made of the new core lava and the talus volumes, but the more widely dispersed and low-lying pyroclastic flow deposits could not be imaged and thus their volumes had to be calculated indirectly. The seismicity associated with rockfall and small pyroclastic flows was monitored and the signal duration of these events, together with some camera-based field observations for calibration, was used as a proxy measure of pyroclastic flow runout distance and volume. Section 2 of this paper discusses the AVTIS observational methods and the techniques employed with the seismicity data. These results are presented in section 3 as a daily aggregated time

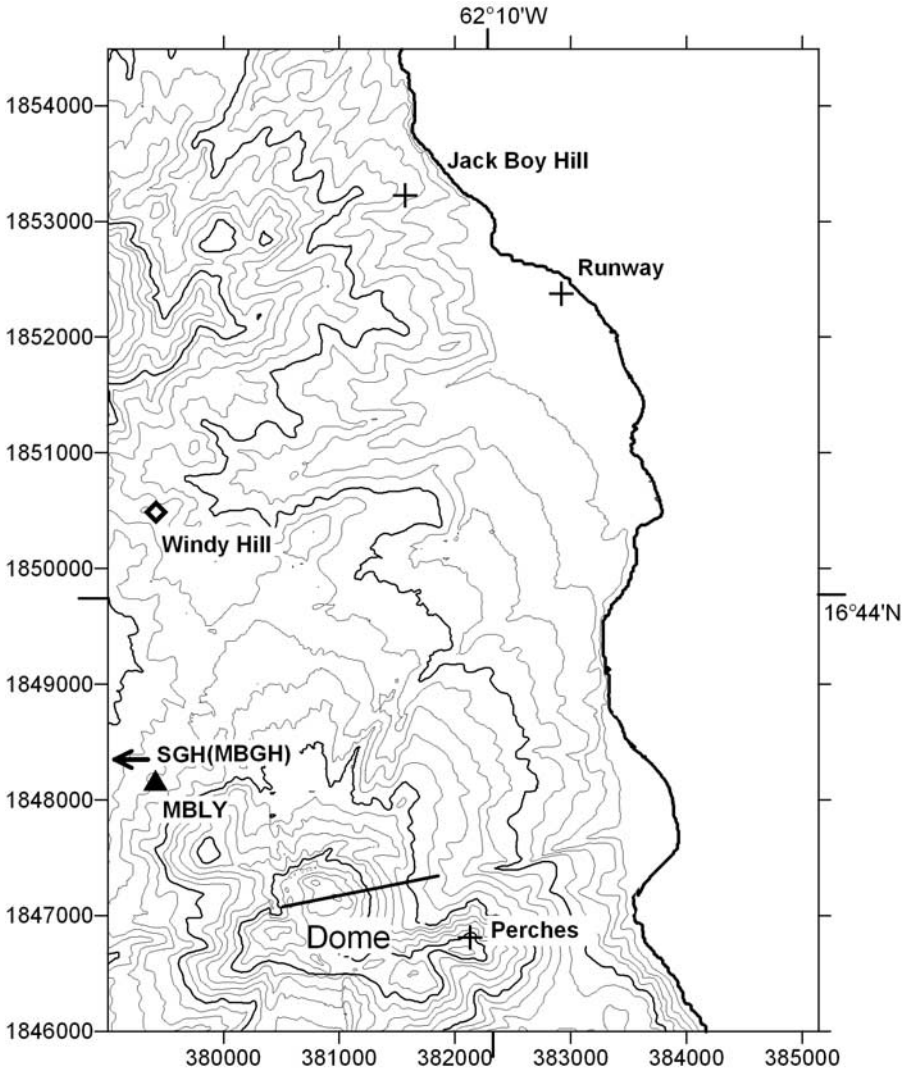

Figure 1. Map of the northeastern slopes of Soufrière Hills Volcano, Montserrat, as of April 2006, showing the locations of AVTIS sites for measurements to the lava dome (crosses), the locations of seismometers MBLY (triangle) and MBGH on St George's Hill (SGH), and the automatic camera at Windy Hill (diamond). Contour interval is 50 m with bold contours at 250-m intervals, and the ticks representing local topographic grid intervals are every kilometer. The line through the dome is the line of the section shown in Figure 2.

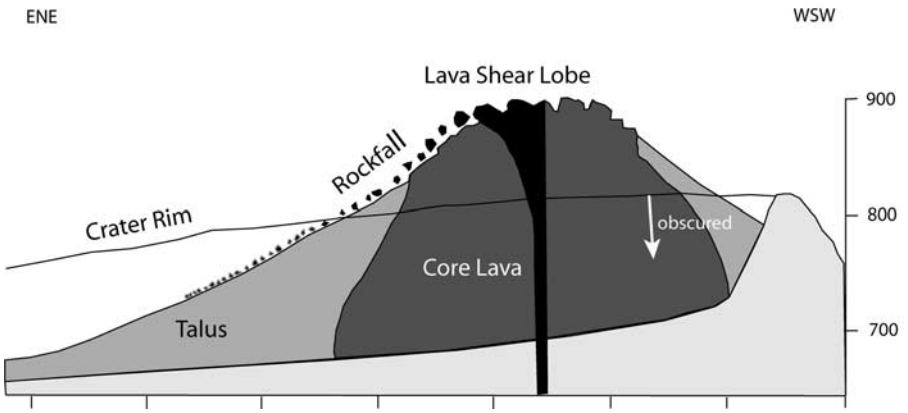

Figure 2. Schematic scale cross section through the Soufrière Hills Volcano lava dome showing the lava shear lobe fragmenting to talus through rockfall. The lower part of this talus is obscured by the crater wall. Right-hand scale is in meters above sea level.

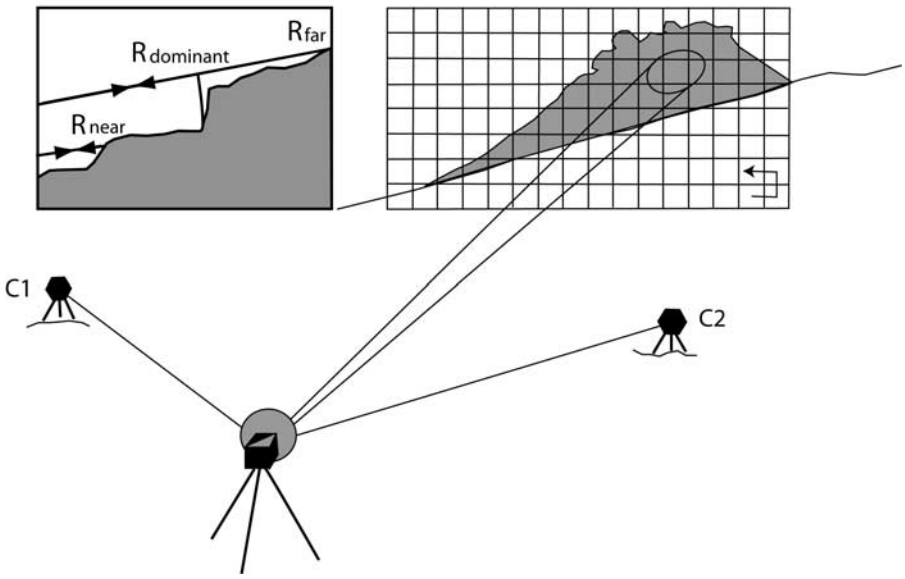

Figure 3. Schematic of the field deployment of AVTIS. The distant lava dome is imaged as a raster built up from the bottom (arrow) using a pan-and-tilt gimbal. C1 and C2 are tripod-mounted corner cube reflectors at distances of several hundred meters used to provide absolute pointing knowledge for AVTIS. The top left panel shows a schematic cross section through the footprint of the radar beam on the dome surface during a single LOS measurement. R_{near} and R_{far} are the near and far ranges of the footprint and $R_{dominant}$ is the dominant reflector whose range will be taken as the range value for that LOS measurement.

series of measurements from which the volumetric budget of the tripartite fractionation of the dome during extrusion and mass wasting is calculated.

2. Observations

2.1. AVTIS

[10] The AVTIS measurements were made from two main sites on the eastern side of the volcano, Jack Boy Hill (JBH) and Runway, both to the north northeast of the dome (Figure 1). From these sites the northeastern sector of the dome and part of the talus slope which was visible above the crater rim in the foreground (Figure 2) could be observed. The direction of lava extrusion during the measurement period was to the east or southeast, so lava extruding near the summit of the dome tended to be pushed out and fell downslope in a dispersed fan of material, some of which became obscured from AVTIS by the crater wall.

[11] AVTIS images topography by measuring the direction and range to the ground surface along a line-of-sight (LOS), taking about 0.25 seconds to send and receive the radar signal, record the data and increment the radar to its next measurement direction, giving an acquisition time of about 20 minutes for a typical 100 by 50 pixel range image. The returned signal received by AVTIS is quantized into 8192 bins and converted into range, with each bin representing 0.85 m. The JBH and Runway sites were the closest ($\sim$6 km) practical, safe, vantage points for multiple occupation, but almost at the operational limit of the instrument ($\sim$7 km). At ranges of $\sim$6 km, the reduction in return signal strength, and hence signal-to-noise ratio (SNR), reduces the accuracy with which the range to the surface can be retrieved. At ranges of $\sim$3 km (as measured, for example, from St George's Hill, SGH; Figure 1) the typical return signal from the volcano has an SNR of about 8.5 dB, resulting in a range uncertainty for a single LOS given by a standard deviation of about 3 m. At ranges of $\sim$6 km, the SNR falls to about -0.35 dB and the range uncertainty increases to about 12.5 m.

[12] The instantaneous field of view of the radar, or footprint, on the volcano's surface is determined by the radar beam width (0.5°), which corresponds to an effective diameter of $\sim$52 m at a range of 6 km. However, because the dome surface is not orthogonal to the radar LOS, the footprint will be larger and noncircular. Within a typical footprint on the dome the individual scatterers (e.g., lava block facets) will be distributed irregularly and will contribute variably to the strength and effective range of the return signal. Filtering of the radar signal to remove the effect of these localized scatters gives a better measurement of the range to the bulk topography [*Macfarlane and Robertson*, 2006] but, at long ranges with low SNR, the range bin chosen to represent the radar footprint can be dominated by the position of the scatterer with the largest radar cross section, rather than that most central to the footprint (Figure 3). Although the radar beam width is 0.5°, the angular stepping used in this study was 0.1° in both azimuth and elevation, and this oversampling helped to reduce the noise in the resulting surface retrieval.

[13] For each site occupation, which typically consisted of several hours of repeated image acquisition with the same instrumental setup, the instrument was set on a leveled tripod at a position known by differential GPS. AVTIS does not have an internal reference for absolute orientation of the

Table 2. AVTIS Deployment[a]

Date	Runway	JBH
30 March 2006	1 (5) 15:53–20:25	
31 March 2006	2 (4) 15:25–18:41	3 (0)
1 April 2006		
2 April 2006		5 (14) 15:10–01:44
3 April 2006	6 (1) 19:20–19:51	7 (8) 22:54–02:14
4 April 2006		
5 April 2006	9 (4) 16:07–19:13	10 (7) 21:51–02:27
6 April 2006	11 (2) 15:34–19:24	12 (5) 20:34–22:43
7 April 2006	13 (3) 16:14–20:17	14 (15) 22:09–07:49
8 April 2006		15 (11) 14:39–22:06
9 April 2006		17 (4) 20:54–23:59

[a]Each site occupation is numbered (in chronological order) with the number of images per occupation given in brackets and time span (UTC) of acquisition periods from different localities.

radar beam, so absolute pointing knowledge was determined using two or more tripod-mounted corner-cube reflectors placed at distances up to several hundred meters from the instrument (Figure 3). These reflectors had their positions measured by differential GPS and were left in the field for the duration of the campaign. The known antenna pattern of AVTIS was identified in the radar data, giving the azimuth and elevation radar coordinates of both reflectors. Comparison with the GPS data then allowed the absolute orientation of AVTIS to be determined. These measurements were performed before and after each AVTIS image acquisition so that the pointing coordinates could be averaged over each site occupation. Analysis shows that the relative accuracy of angular referencing within each occupation is about 0.01°, confirming the stability of the platform, and the reproducibility of the pan and tilt gimbal. However, between repeat occupations of the same site, resetting of the tripod results in reduced repeatability and small systematic offsets in the extracted surfaces. These offsets were removed by refining the calculated instrument orientations in order to minimize the differences between surfaces retrieved from stable terrain. Here, we used the outer, north-facing slopes of the volcano below the crater rim (an area of 0.1 km^2 and slope of about 25°, at a range of about 5 to 5.5 km) and, after pointing refinement, the results show elevation standard deviations of about ±3 m, when adjusted to their optimum fits.

[14] The reflector measurements also provided range benchmarks from which any drift in the radar range measurement could be assessed and corrected. The slope of the radar frequency sweep, which determines the received frequency to range conversion, was found to vary slowly over the course of a site occupation, as the instrument changed temperature. After initial warm-up, the range accuracy would typically drift by up to 0.05% over the course of a single scan—i.e., a maximum drift of ~3 m at 6 km range. Over a complete site occupation of several hours, the range of drift could total as much as 0.5% (30 m at 6 km range). The GPS-measured reflector positions were therefore used to calibrate the range drift based on the apparent radar range at the start and end of each scan.

[15] Consequently, individual AVTIS range measurements during this campaign were subject to inaccuracies arising from low signal strength, drift, local scattering effects and pointing uncertainties. The resultant noise in the range data, which was dominated by the low SNR at long ranges, was reduced by temporal stacking of range profiles within each site occupation, giving a daily average for the two sites, when occupied (Table 2). The resultant occupation-averaged range values were then combined with absolute orientation data to provide 3D coordinates of surface points that were then interpolated spatially onto a 10-m grid (Montserrat local grid coordinates) by kriging. Temporal stacking in this way means that any topographic changes during the period of the occupation will be averaged, and the resulting surfaces are assumed to represent the dome surface at the midpoint of each occupation.

2.2. Rockfall Seismicity

[16] Montserrat Volcano Observatory (MVO) maintains a record of rockfall-induced seismic events consisting of the time, duration, repose interval and energy release for each recorded event, as derived from its broadband network of seismometers. However, a large number of smaller volume rockfalls impart too little energy to the ground to be recorded as a network event, so only the largest magnitude rockfalls are recorded in the seismicity catalogue. The energy (actually the energy density in $J \cdot kg^{-1}$) measured for each event varies with instrument and location and can be used to locate the travel paths of flows [*Jolly et al.*, 2002]. We have used mainly data from the MBGH seismometer, located about three kilometers west of the dome. For part of 9 and 10 April we have also used the MBLY seismometer record, which was the only instrument operating during that interval. By calibrating MBLY against MBGH we have substituted the appropriately scaled MBLY data for 9/10 April into the MBGH record. We justify this on the grounds of the similarity of the energy characteristics measured at MBLY over the two periods.

[17] MVO distinguishes between rockfall (RF) and long-period rockfall (LPRF) events, with RF events characterized by high-frequency spectra (2–8 Hz) and LPRF events having an additional spectral peak in the 1- to 2-Hz range. This long-period component originates from fluid resonance in the conduit and is sometimes associated with gas releasing into the atmosphere, particularly when the extrusion rate is high [*Luckett et al.*, 2002]. *Calder et al.* [2005] showed that, for rockfall data for the 1995–1997 period, with increased extrusion rate of lava (and particularly for higher rates), the duration of each seismic event increased and the repose interval decreased.

[18] It is possible to use the rockfall seismic event catalogue to infer flow volumes by examining the correlation between seismic event duration and observed flow runout distance (Figure 12a) and then converting distance to flow volume. To determine runout distance, several types of photographic information were used to estimate the runout of rockfalls and pyroclastic flows as measured from their sources near the summit of the dome. These included hand-held, and tripod-mounted, still and video cameras at the AVTIS measurement sites, and the MVO automated camera at the Windy Hill site (Figure 1) that captured images every minute and was available from 1 to 10 April. The distal extent of the rockfalls and flows generally could not be seen directly in these images, but their locations were inferred (to the nearest 100 m) from the image positions of the turbulent buoyant ash plumes that the flows generated

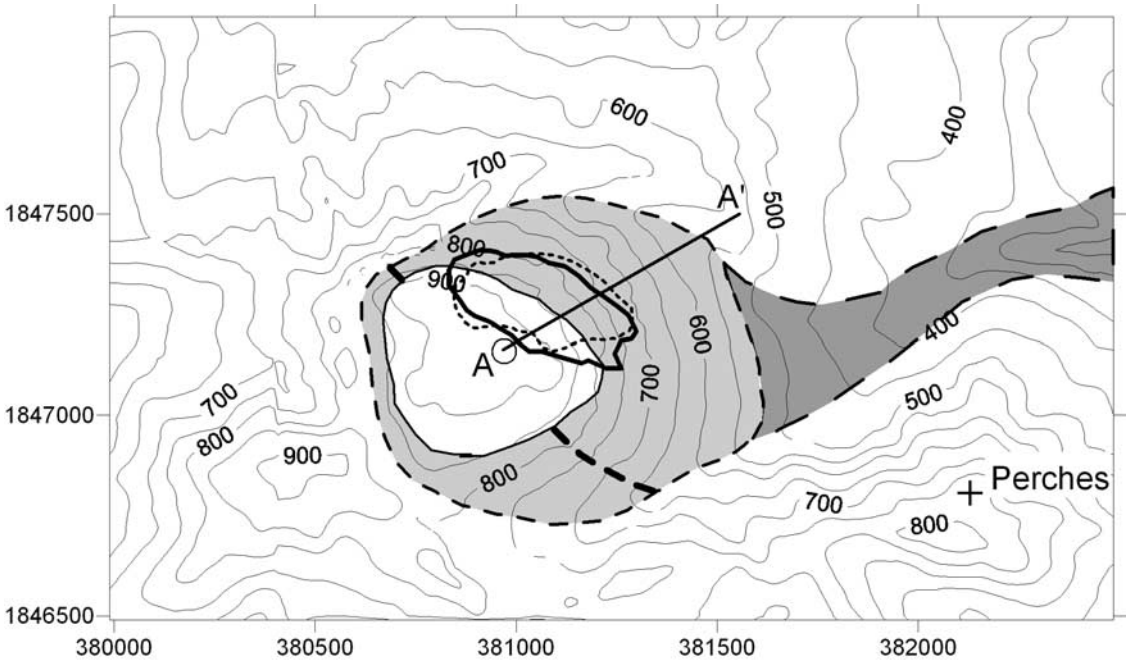

Figure 4. Map of the dome and crater. The fine dashed and thick solid lines denote the approximate areas on the dome covered by AVTIS from the JBH and Runway sites, respectively. The area of the dome covered by lava is shown in white, the area covered by talus in light gray, and the area of pyroclastic flow deposits in dark gray. The thick dashed line denotes the southwestern boundary of active mass wasting. The position of the vent for the dome is shown by the circle, the solid line leading from it is the line of the profile A–A′ in Figure 7. Contours are shown every 50 m asl.

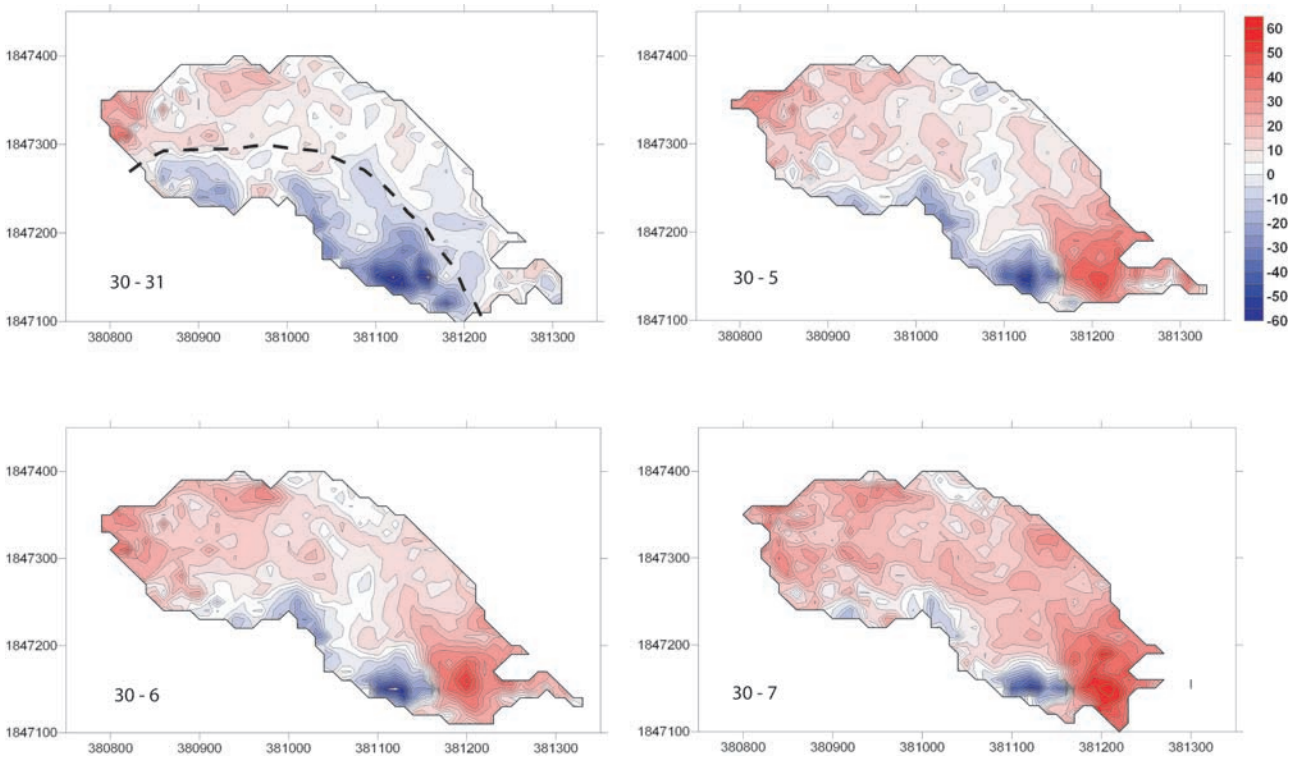

Figure 5. Changes in the surface elevation of the lava dome measured from Runway between the dates shown (e.g., 30–31 is the difference between 30 and 31 March 2006). The elevation change scale is in meters, contoured at 5-m intervals. The dashed line in the 30–31 panel represents the approximate position of the lava/talus boundary.

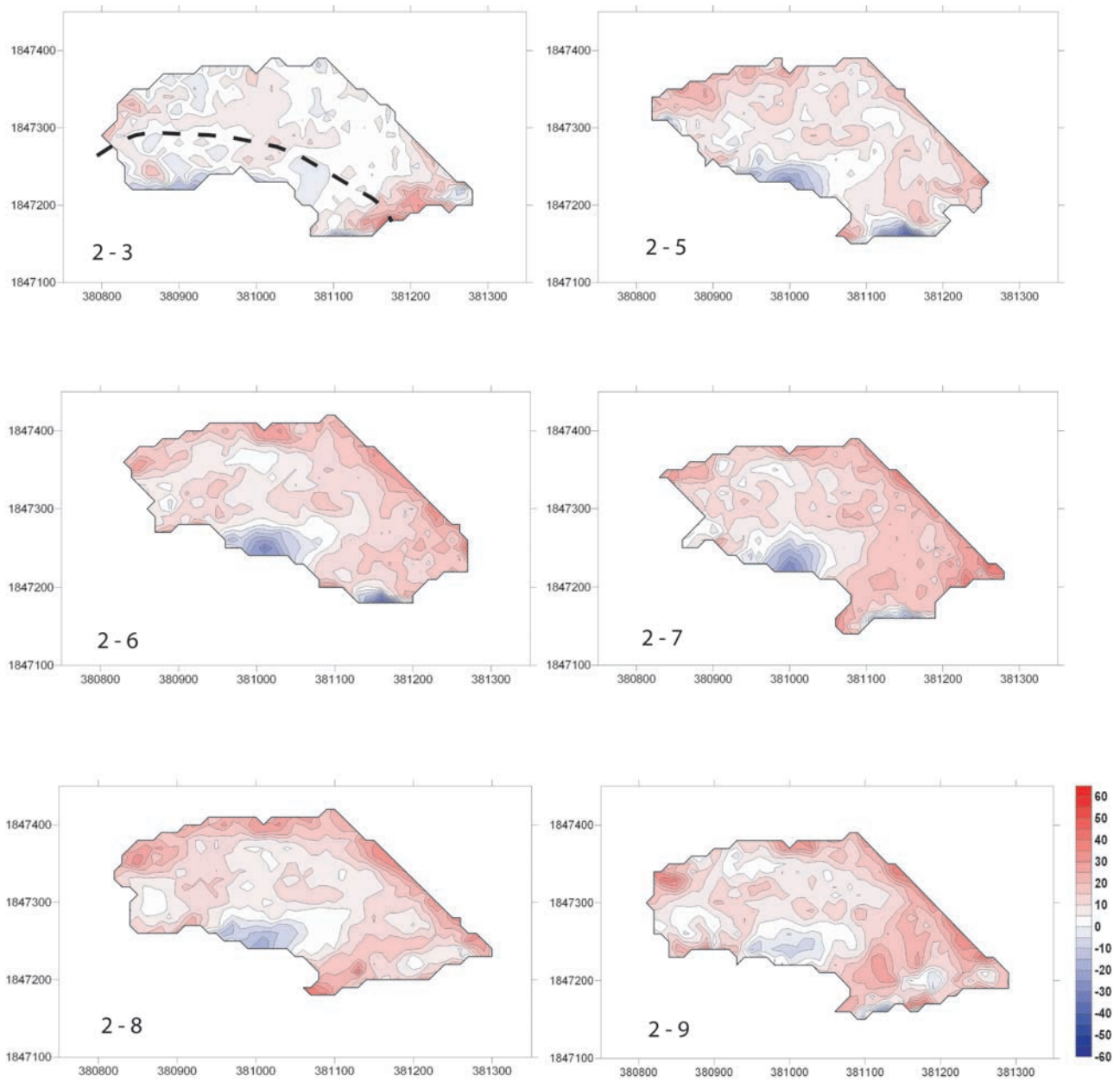

Figure 6. Changes in the surface elevation of the lava dome measured from JBH between the dates shown (e.g., 2–3 is the difference between 2 and 3 April 2006). The elevation change scale is in meters, contoured at 5-m intervals. The dashed line in the 2–3 panel represents the approximate position of the lava/talus boundary.

relative to the background topography. The flow runout values generated in this way are likely to be underestimates in some cases because the wind was almost always from the east during this period, moving in the opposite direction to the majority of flows, and tended to blow the ash plumes westward, back from the flow front, as they rose. The one-minute interval images were more susceptible to this effect, the video data less so.

[19] To convert runout lengths into deposit volumes, typical values for the other deposit dimensions are required. Field observations of flow deposits at Soufrière Hills that extend just beyond the talus typically show variations between thin (0.2 m thick), sheet-like (100 m wide) deposits to channelized/lobate deposits (10–30 m wide; 0.5–2 m thick) [*Cole et al.*, 2002; Figure 9a] giving cross-sectional areas in the range 5–60 m^2. *Calder et al.* [2002] suggested volumes up to 1000 m^3 as typical for rockfalls with runouts up to 500 m. Using the above range of cross-sectional areas, the volumes of deposits at 1 km runout would be 5,000–60,000 m^3. 10,000 m^3 for 1 km runout deposits was suggested by *Calder et al.* [2002]. For flows up to 2 km runout, volumes of up to about 100,000 m^3 have been estimated [*Cole et al.*, 2002]. Consequently, each RF/LPRF event with a runout greater than 500 m (based on duration) is assigned a volume using a linear fit to the three runout-volume values: 10^3 m^3 at 500 m, 10^4 m^3 at 1000 m and

Table 3. Cumulative and Daily Averaged Volumetric Differences Between the Surfaces Measured by AVTIS From the JBH and Runway Sites

	JBH			Runway		
Date	Occupation	Cumulative Volume (10^3 m^3) [Area 10^3 m^2]	Daily Volume (10^3 m^3)	Occupation	Cumulative Volume (10^3 m^3) [Area 10^3 m^2]	Daily Volume (10^3 m^3)
30 March 2006				1	0	
31 March 2006				2	−13 [76]	−13
1 April 2006						148
2 April 2006	5	0				148
3 April 2006	7	339 [63]	339			148
4 April 2006			76			148
5 April 2006	10	490 [58]	75	9	727 [74]	148
6 April 2006	12	772 [63]	282	11	1029 [72]	302
7 April 2006	14	818 [58]	46	13	1240 [75]	211
8 April 2006	15	875 [67]	57			
9 April 2006	17	872 [64]	−3			

10^5 m^3 at 2000 m. We estimate the uncertainties on the resulting volumes to be in the range 50–100% at a minimum.

3. Results

3.1. AVTIS

3.1.1. Talus Volumes From Topographic Surface Changes

[20] The JBH and Runway viewpoints image slightly different areas of the dome. From Runway, more of the southeastern sector of the dome is seen but, being lower in elevation than JBH, more of the lowermost talus is obscured by the crater wall. The average area of the dome covered by AVTIS from both viewpoints is about 700,000 m^2, with a spatial density of range points of about 1 per 100 m^2. Due to instrument repositioning between repeat site occupations, no two data sets represent precisely the same lines of sight, but Figure 4 shows the maximum areas covered from the two viewpoints. Both compose about 50% lava surface in the southwest and 50% talus in the northeast. Figure 4 also shows that a sector of about 180° was thought to be actively involved in mass wasting during this period (Figure 11).

[21] Figures 5 and 6 show the surface differences for each successive occupation for JBH (relative to 2 April 2006) and Runway (relative to 30 March 2006) sites, respectively, and Table 3 gives the net volumetric changes and areas of overlap used to calculate those changes. With two exceptions, successive differences show net increases in volume. From Runway, the uppermost southeastern part of the dome shows a large negative area developing between 30 and 31 March. Five days later on 5 April, the negative feature is reduced in magnitude and area and a large positive feature has formed immediately to the east. In the succeeding two days (6 and 7 April) this trend continues. We interpret the negative feature to be the result of a large collapse event, removing 40 m or more of dome lava from around the summit and moving it out of the measurement area.

[22] There were no equivalent measurements from JBH on 30 and 31 March, and the coverage from JBH includes only the northernmost parts of the two main features measured from Runway. A distinct negative feature can be seen in the JBH data on the south central part of the dome (Figure 6). Like the Runway data, most of the new talus volume is added to the lowermost eastern slopes. There was a negligible change in measured talus volume between 8 and 9 April. As we shall see, this was a period of increased pyroclastic flow activity and it may be that this low net volume was because the rockfall transport was particularly effective in moving it away from the upper talus slopes. The uncertainties on these estimates must be higher than those for the outer crater differences (±3 m), mainly due to difficulties in the precise determination of the dome "horizon" due to the radar beam width. They cannot be independently quantified and an uncertainty level of ±5 m is used.

[23] The average rate of height increase of the surface (Figures 5 and 6; Table 3) is about 2.0 m per day; 14 ± 5 m over 7 days for JBH, and 17 ± 5 m over 8 days for Runway. The volumetric rate of addition for these two intervals is 1.4 m^3·s^{-1} for JBH and 1.9 m^3·s^{-1} for Runway. However, a considerable portion of the talus and the volume that must have accumulated there is hidden from both viewpoints. The profiles through the Runway surfaces for 30 March and 7 April (Figure 7) indicate these hidden accumulations.

[24] The volume of the new talus hidden from AVTIS during the measurement period (Figure 7) can be estimated

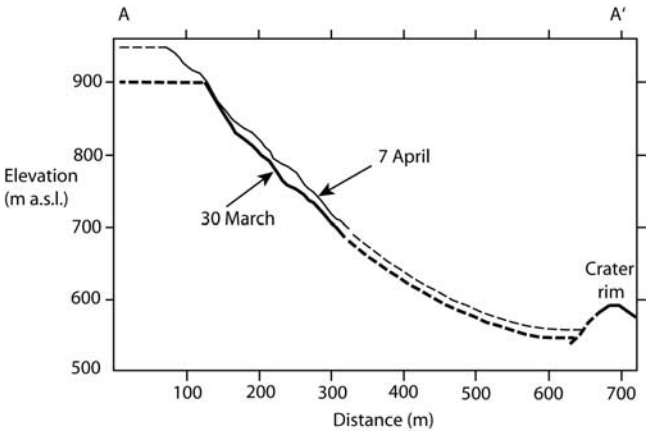

Figure 7. Comparison of two profiles through the surfaces measured by AVTIS from Runway on 30 March and 7 April. The dashed portions of the lines are inferred. The orientation of the profile is shown by the solid line A–A′ in Figure 4.

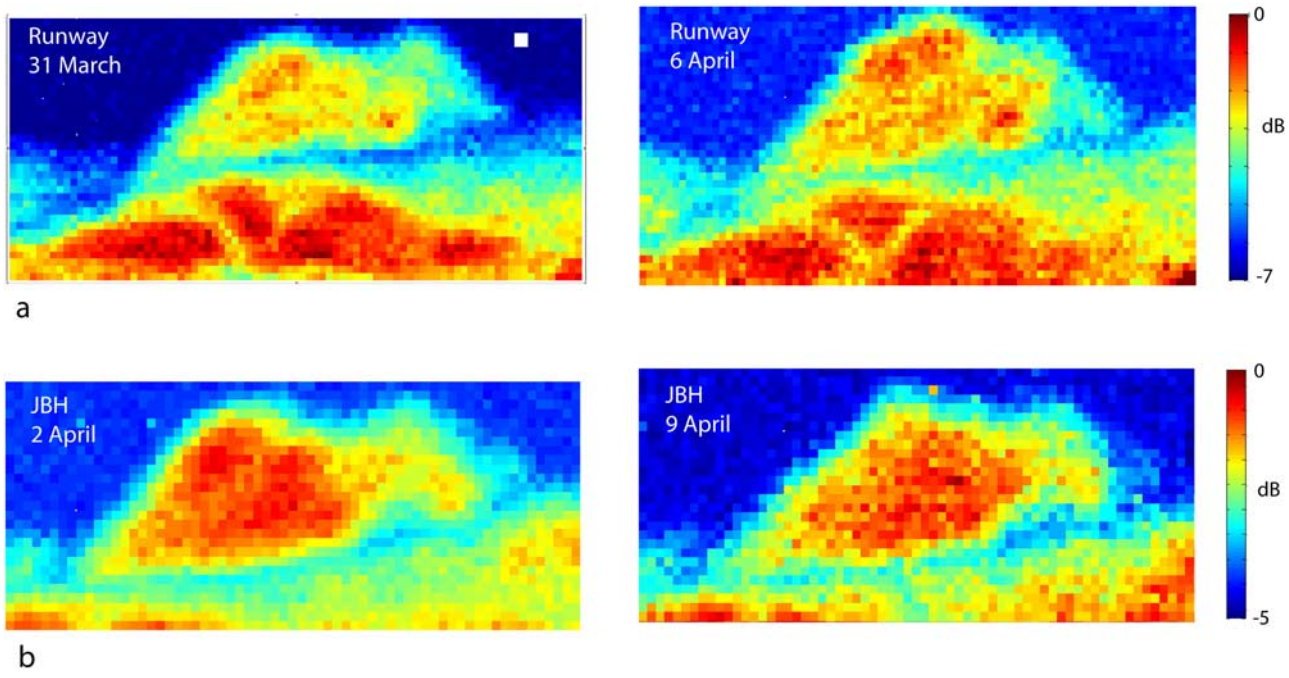

Figure 8. AVTIS intensity images of the lava dome. Figure 8a shows the averages of intensity collected in occupations 2 (30 March) and 11 (6 April) from the Runway site. Figure 8b shows the averages of intensity collected in occupations 5 (2 April) and 17 (9 April) from the JBH site. Variations in cloud cover from occupation to occupation meant that the absolute reflectivity values for the surface could not be determined. The color scales therefore represent relative reflected power intensity scaled for each particular occupation: a 7-dB range for the Runway images and a 5-dB range for the JBH images. The pixels on the dome represent areas of about 10 × 10 m.

for the region actively involved in mass wasting, which has an area of about 0.4 km^2 (Figure 4). AVTIS surface differencing accounted for the volumetric change over areas of about 0.07 km^2 from both Runway and JBH sites (Table 3), about 17% of the total, active area. We now assume that the daily volumetric changes measured by AVTIS, averaged when there is near-contemporaneous Runway and JBH data (Table 3), can be extrapolated to the whole of the area of active talus in proportion to the areas concerned (Table 5). The total talus volume thus produced is 7.2×10^6 m^3. This may be an underestimate because much of the extrapolated area is at lower elevation and thus there are relatively fewer "source" areas of mass loss from the upper part of the dome. The extrapolated area also has a generally lower gradient than the AVTIS-measured areas and so deposition should be more likely. On the other hand, use of the observed areas may have overestimated the volume deposited in the south.

[25] To compare the proportion of lava staying in the dome core to that deposited as talus or in pyroclastic flows, bulk volumes need to be converted to their dense rock equivalents (DRE). *Sparks et al.* [1998] used bulk densities of 2600, 2250 and 2000 $kg \cdot m^{-3}$ for dense rock, vesicular lava and pyroclastic flow deposits at Soufrière Hills and corresponding density ratios of 0.86 and 0.77 for converting bulk vesicular lava and pyroclastic flow deposit volumes to DRE. Density ratios for bulk clastic rocks fall in the range 0.65–0.60 (mean 0.63) (e.g., www.simetic.co.uk/si_materials.htm). An appropriate figure for the density ratio for Soufriere Hills talus might be 0.54 (0.63 × 0.86), though this would be a minimum value because infilling with fine ash is not taken into account. In the following calculations we use the ratios of 0.86, 0.77 and 0.54 to normalize the bulk volumes of core lava, pyroclastic flow deposits and talus, respectively. Thus the DRE for the total talus volume is 3.9×10^6 m^3.

3.1.2. Dome Core Lava Volumes From Intensity Measurements

[26] The strength (intensity) of the signal received by AVTIS is a function of the range distance, path attenuation, the local scattering and dielectric properties of the surface (reflectivity), and the angle that the surface makes with the radar beam. Typically, the variability of the intensity across the dome's surface is about 3–4 dB at a range of 6–7 km. *Macfarlane et al.* [2006] were able to distinguish the highly reflective, blocky, surfaces of new lava flows from less reflective ash-covered surfaces at a distance of about 3 km using AVTIS intensity images of Arenal volcano. No similar distinction is apparent at Soufrière Hills, where the talus and lava surfaces tend to exhibit similar intensities. Fortuitously oriented, large (>10 m), blocks of lava often give stronger intensities than their surroundings, and the continuity of some of these can be tracked in the time series over several days. *Anderson et al.* [1998] proposed that the block size of silicic lava flows in the range 0.2–5 m was inversely correlated with extrusion rate. Unfortunately, the footprint of the radar at the dome from JBH and Runway is too large to resolve local roughness (via a root mean square measure of intensity) at that length scale.

Table 4. Maximum Dome Elevations and Incremental Summit Lava Volume Estimates Derived From AVTIS Data Collected at Runway and JBH Sites

Date	Maximum Elevation From Runway (m asl)	Maximum Elevation From JBH (m asl)	Summit Lava Volume Increment From Runway (10^3 m^3)	Summit Lava Volume Increment From JBH (10^3 m^3)
30 March 2006	910			
31 March 2006	910		35	
1 April 2006				
2 April 2006		920		
3 April 2006		910		−422
4 April 2006				
5 April 2006	920	910	246	317
6 April 2006	950	940	1020	651
7 April 2006	950	940	229	88
8 April 2006		930		475
9 April 2006		940		264

[27] While the intensity data cannot be employed statistically, we can use them to quantify the volume of lava at the top of the dome. The skyline of the dome viewed by AVTIS from JBH or Runway has a diminishing intensity as increasing amounts of "sky" dilute the return signal from the dome. Nevertheless, the AVTIS-derived intensity skyline yields useful information about the elevation profile of the summit of the dome and from that the component of the lava output that remains as part of the dome core. Figure 8 shows a pair of intensity images from both measurement sites. Over the eight-day and seven-day intervals separating the images in the two pairs, major changes have occurred. The elevation of the more easterly of the two peaks has grown and the gradient of the more southeasterly profile (to the left of each image) has reduced slightly with time. From such images, the equivalent elevations of the surfaces derived from the range data and from photographs, we have estimated the changing summit profiles with time. The highest parts of the dome measured by AVTIS from the daily surfaces are shown in Table 4 to the nearest 10 m. Between 5 and 6 April the dome increased its maximum elevation from between 910 and 920 m asl to between 940 and 950 m asl. There seems to have been no further increase measured after that up to 9 April. On 18 May 2006 the elevation of the dome summit was surveyed by total station as 1006 m asl.

[28] From the daily average intensity images of the dome (four examples are shown in Figure 8) and the range data, measurements of the areal increments of lava added to the summit (Figure 7) along the AVTIS LOS have been made for each occupation (Table 4). Note that we cannot use the range-derived surface differencing method here because, generally, the summit data do not overlap in the LOS (Figure 7). Lack of observations of the western side of the dome summit prevents an accurate measurement of the whole summit area. Nevertheless, we can estimate the incremental volumes of lava added and lost to the summit by assuming that each observed profile is representative of a 200-m diameter cap of lava. These estimates are shown in Table 4. Uncertainties of about 30–50% are considered likely. Given that most of the lava extrusion was directed toward the eastern side of the summit, this assumed radial symmetry means that the volumes may be over-estimated. The volume of lava remaining at the summit increased generally in a similar way in both data sets, though at a faster rate later in the measurement period. The exception is the interval between 2 and 3 April for the JBH record, when a net reduction in height was recorded. This implies a significant collapse volume for this interval. Table 4 shows that both data sets record a notable increase in lava added between 5 and 6 April. Averaging the two data sets gives a total addition to the summit of about 1.7×10^6 m^3 (1.5×10^6 m^3 DRE) of lava over the eleven-day interval from 30 March to 9 April.

3.2. Pyroclastic Flow Deposit Volumes From Rockfall Seismicity

[29] The number of recorded RF and LPRF events during the AVTIS campaign increased at the start of the measurement period from a lower level, dipped on 5/6 April, and peaked on 8 April (Figure 9) with their proportions remaining nearly constant. However, the seismic energy released varied greatly (Figure 10), with several large magnitude events occurring on 31 March, and the largest single energy

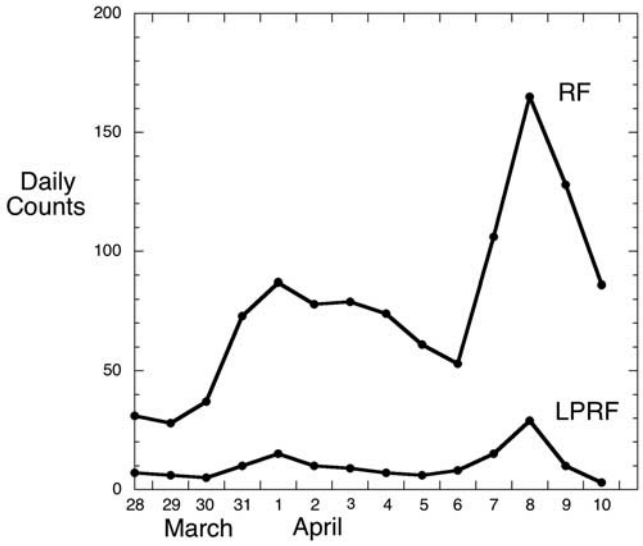

Figure 9. Number of RF and LPRF events recorded on the MVO seismic network each day between 28 March and 10 April 2006.

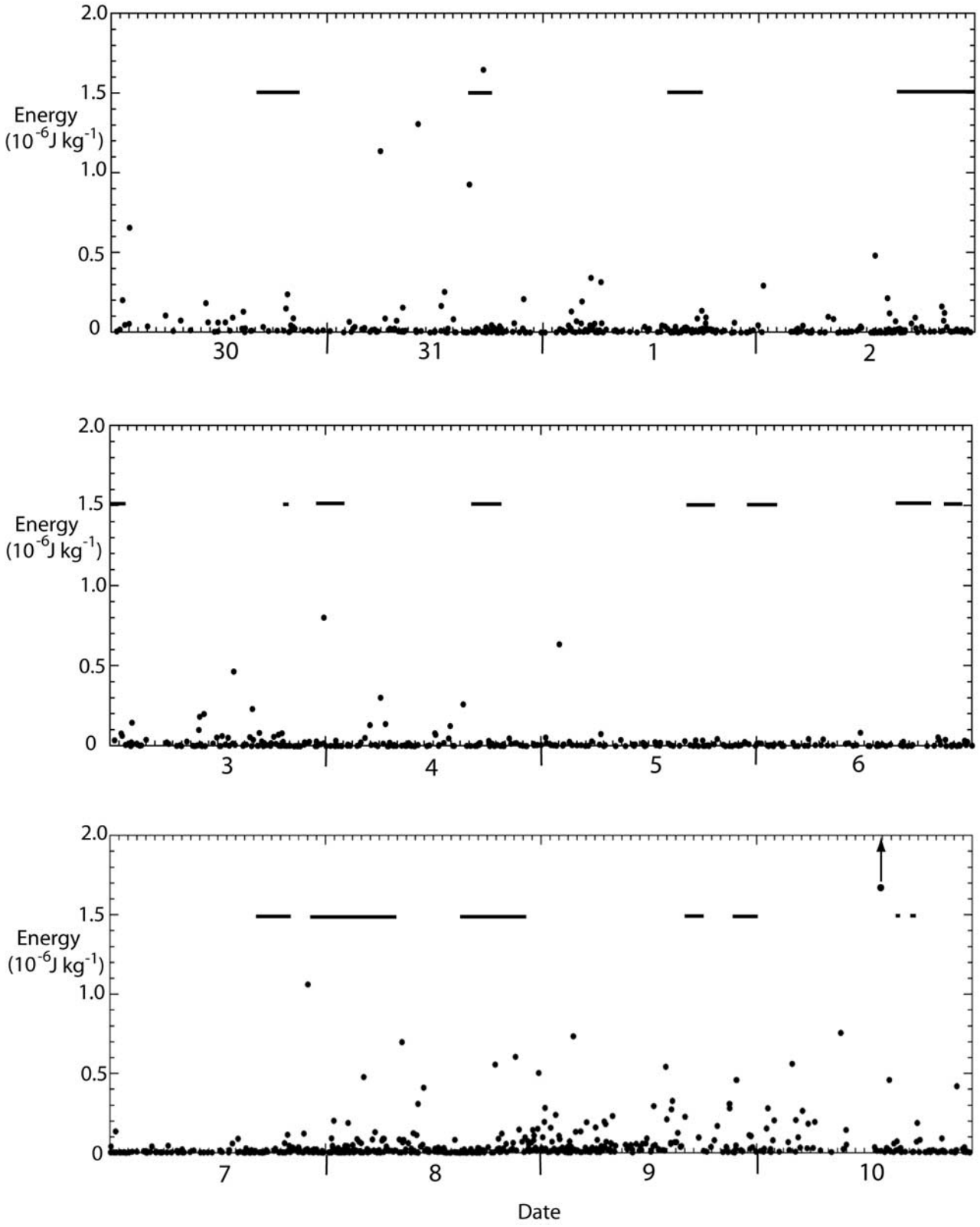

Figure 10. Time series showing the magnitude of energy release by individual RF and LPRF seismic events (black dots) between 30 March and 10 April 2006 (measured from station MBGH at St George's Hill as the energy density (square of the seismic velocity) in $J \cdot kg^{-1}$). The black bars are the durations of the AVTIS range measurements. Times are in UTC. The off-scale event on 10 April denoted by the arrow had an energy of 9.1×10^{-6} $J \cdot kg^{-1}$. The data between 0800 h on 9 April and 1300 h on 10 April are data from station MBLY calibrated to MBGH energy levels.

Table 5. Daily Volumetric Budget for Lava, Talus, and Pyroclastic Flow Deposits

Date	AVTIS Area Volumes (10^3 m^3)	Active Talus Volumes (10^3 m^3)	Summit Lava Volumes (10^3 m^3)	Pyroclastic Flow Volumes (10^3 m^3)	Daily Total (10^3 m^3)
30 March 2006	–	–	–	39	39
31 March 2006	−13	−68	35	58	25
1 April 2006	148	800	49	180	1029
2 April 2006	148	800	49	109	958
3 April 2006	243	1409	−373	249	1285
4 April 2006	111	673	49	111	833
5 April 2006	111	673	183	73	929
6 April 2006	292	1743	836	71	2650
7 April 2006	129	770	159	162	1091
8 April 2006	57	337	475	508	1320
9 April 2006	−3	−19	264	281	526
Totals	1223	7206	1726	1841	10685

release event on 10 April (Figure 11). Some of these events were observed to correspond to the generation of pyroclastic flows but the period 5–7 April was notable for a lack of larger magnitude events. The longest runout pyroclastic flow that was observed visually reached 1800 m from the dome summit at about 14:30 UTC on 2 April.

[30] Almost all the 70 visually observed events could be correlated with the equivalent seismic record, which contained a total of 1053 RF and LPRF events. The disparity between these two figures is largely accounted for by lack of visual observations during the night and during periods when cloud covered the volcano. Pyroclastic flows could sometimes be observed emerging below the cloud base, whereas rockfall events at that time would be unobserved visually. Using the rockfall seismicity duration data (Figure 12) allowed the total volume of pyroclastic flows for the 30 March to 9 April period to be estimated as 1.8×10^6 m^3 (1.4×10^6 m^3 DRE).

3.3. Temporal Variability

[31] Combining the DRE estimate of pyroclastic flow deposit volume (1.4×10^6 m^3) with the estimates for the talus volume (3.9×10^6 m^3) and summit lava (1.5×10^6 m^3) gives a total of 6.8×10^6 m^3 for the eleven-day period (Table 5). Figure 13 shows the cumulative daily totals for the talus, talus-plus-summit-lava and all three sources together. Up to 5 April the output is nearly linear. Note that the net loss of lava from the summit between 2 and 3 April (Table 4) moves the talus-plus-summit-lava curve below the talus curve until 5 April. After 5 April the contribution from the summit lava increases and the overall output rate increases. The equivalent daily seismic energy release shows a different pattern (Figure 13), with a gradual reduction from 31 March to 6 April, followed by a much higher rate. Both data sets show the same contrast between modest rates in the first part of the record and the much more vigorous second period. The main difference is that the volumetric estimates show a rise on 5 April, while the inflection in the cumulative rockfall seismic energy occurs on 7 April. Our interpretation of this is that the lava supply rate increased on 5 April. This had the effect of building up a new mass of lava at the summit, as observed by AVTIS. Rockfalls that occurred were smaller than usual and fewer were recorded as events from the seismometer network. For 5 and 6 April the rockfall seismicity was not a good proxy for the high lava extrusion rate, but from 7 April onward the size and number of rockfall events increased greatly as the high rate of extrusion was maintained. It is possible that this lag in behavior was due to the reorientation of the extrusive vent.

4. Discussion

[32] The summit of the lava dome was either in cloud or darkness for about 90% of the campaign. Nevertheless, opportunistic photographs taken from the AVTIS measurement sites confirm that the lava dome changed its shape and size during the AVTIS observation period. The summit of the dome increased its elevation, at least one large dome block collapsed and the surface of talus increased its elevation. This talus growth occurred on the eastern side of the dome. Photographs from the Perches site (Figure 11) on 23 March and 10 April show this clearly. Over that eighteen-day period, the talus increased its extent to the southeast, burying an area of fumarolic activity. When this lateral spreading of talus occurred is not certain, the increased rate of rockfall and the large collapse events on 31 March make this a likely contender for the start of this change. A rise in the general elevation of the talus can be seen in Figure 11, particularly along the retaining wall on the northeastern side of the crater.

[33] Photogrammetric surveys of the dome from the east were undertaken by MVO, using sites at Perches and Galway's Mountain (on the crater rim to the west southwest of Perches) on 23 March (Figure 11) and 26 April. These yielded dome volumes of 56×10^6 m^3 and 78×10^6 m^3, respectively (±20%). These estimates include the talus component of the dome, which is more visible from these two sites than from JBH and Runway (Figures 4 and 11), but not the pyroclastic flow deposits further down the valley. The ratio of core lava to talus was not estimated in these surveys. If we assume the same ratio as for the AVTIS survey, this gives an average DRE extrusion rate of 4.9 m^3·s^{-1}.

[34] From the AVTIS measurements and the surface differences generated (Figures 5 and 6) it is clear that between 30 March and 9 April: (i) the summit of the dome rose, (ii) some large masses of the dome lava collapsed, and (iii) the lower talus slopes generally rose by deposition. While there is evidence of talus deposition around most of the observed slopes from the north to the southeast, the

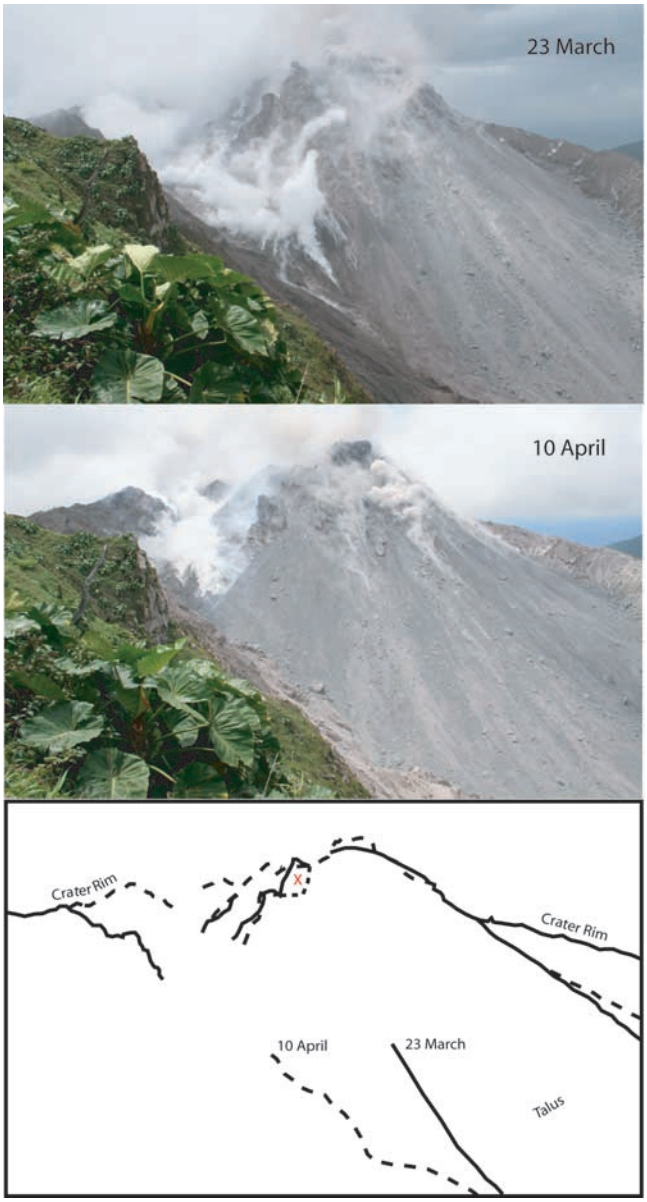

Figure 11. Photographs of the dome from the Perches site (Figure 1) on 23 March 2006 and 10 April 2006 and a sketch of the margins of the dome and talus on the two dates to emphasize the changes. X shows the location of a large mass of dome lava that disappeared after 23 March.

southeastern sector received most of the talus in the second half of the field campaign. This agrees with the photographic observation above.

[35] The proportion of extruding lava that remained within the lava core of the dome from 30 March to 9 April 2006 was about 22%. How certain is this result in the context of the measurement uncertainties? We measured the uncertainty of surface retrieval near the dome as ±3 m, which we relaxed to ±5 m for the dome itself. Over the eleven days of measurement this represented ±25% of the measured change. The estimates of core lava are based on AVTIS range values near the skyline of the dome which are known to be noisy, and we suggested an uncertainty range of ±30–50%. Pyroclastic flow deposit volumes are less well constrained because the rockfall seismicity is a crudely calibrated proxy for volume, and we assigned a ±50–100% uncertainty range. If we take uncertainties of ±25, 40 and 75% to be representative of talus, core lava and pyroclastic flow deposit volumes, respectively, then the proportion of the core to the total has a mean and uncertainty bounds of 22 (11–39) %. The equivalent bounds for talus are 57 (39–80) % and 21 (5–39) % for the pyroclastic flow deposits. Even at the most favorable limit of uncer-

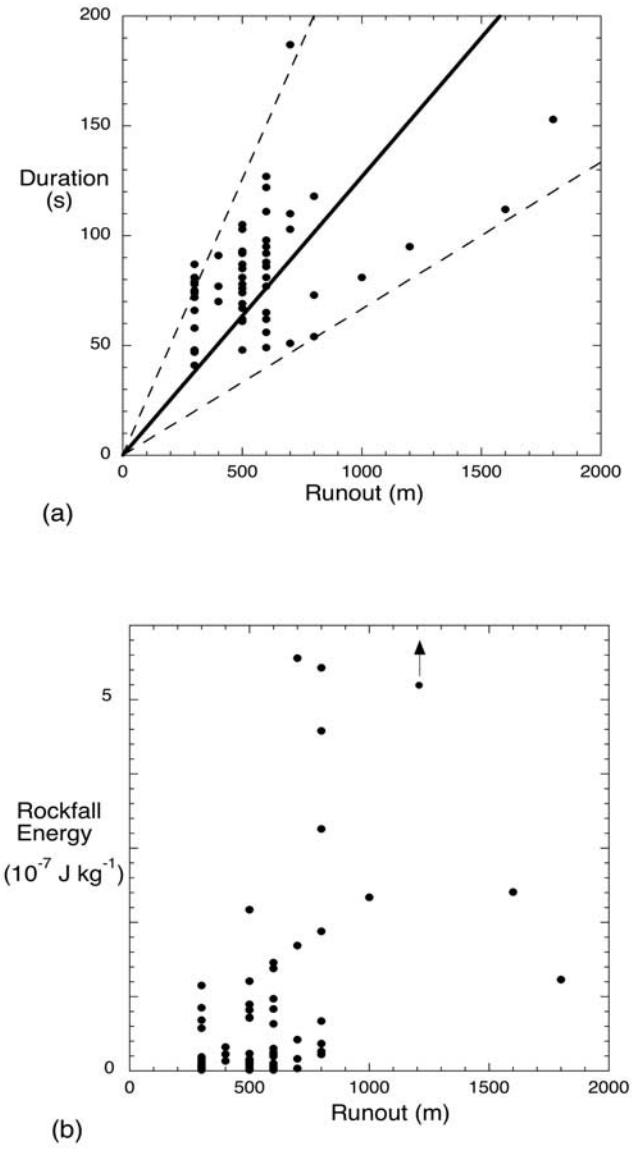

Figure 12. Observed pyroclastic flow runout distances plotted against (a) the signal duration recorded by the seismometer network and (b) the energy release measured at station MBGH (the arrowed event has an energy of 1.7×10^{-6} J·kg^{-1}). The solid line in Figure 12a represents a velocity of 8 m·s^{-1}, and the dashed lines (4 and 15 m·s^{-1}) indicate the limits of video-based estimates of pyroclastic flow velocities beyond the talus. Note that rockfalls observed to remain within the limit of the talus (~500 m) have all been assigned an average runout of 300 m.

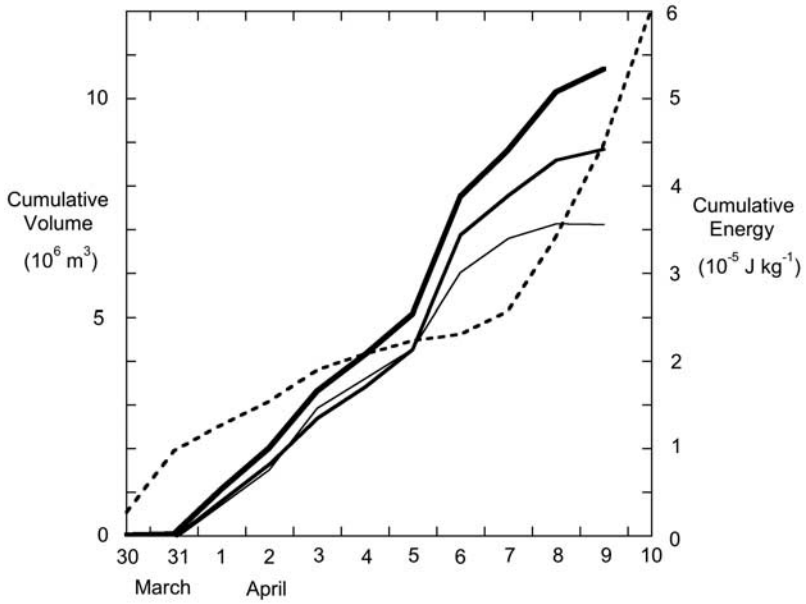

Figure 13. Cumulative daily volumes of talus (thin solid line), talus and summit lava (medium solid line), and talus, summit lava, and pyroclastic flow deposits (thick solid line). Values are from Table 5. Also plotted as the dashed line is the cumulative seismic energy from the MBGH station.

tainty, the lava retained within the core was only slightly more than one third of the total (~39%) and thus the primary finding of this work, that a surprisingly low proportion of extruded lava remained in the core of the dome, is valid, despite the uncertainties. The occurrence of one or two larger collapses and pyroclastic flows, of which there were none in this interval, would change this figure significantly. Nevertheless, we regard the relative fractions involved in mass wasting as being broadly representative of the behavior between these larger collapse events.

[36] This third episode of dome growth (which began in August 2005) was less prone to larger collapse events than during the earlier two episodes of extrusion. For example, during the first half of 1997, when the lava extrusion rate was less than 5 $m^3 \cdot s^{-1}$ the dome:pyroclastic flow volume ratio was about 60:40, but this became about 40:60 when the extrusion rate rose to about 10 $m^3 \cdot s^{-1}$ during the second half of 1997 [*Sparks et al.*, 1998]. This contrasts strongly with the 79:21 ratio measured here during similar extrusion rates. The average DRE extrusion rate over the eleven days was ~7 $m^3 \cdot s^{-1}$, and for the nonpyroclastic flow components a rate of ~5 $m^3 \cdot s^{-1}$, compared to the equivalent ~5 $m^3 \cdot s^{-1}$ measured by photogrammetry for the 23 March–26 April period.

[37] The high proportion of extruded lava that is converted to talus revealed by this study has implications for hazard analysis. Lava that remains in the core of the dome can retain much more heat and gas content and sustain greater overpressures than the surrounding apron of lava talus. The sudden depressurization of this lava can lead to the generation of large, mobile pyroclastic flows and even lateral blasts [e.g., *Woods et al.*, 2002]. Thus, if the high degree of conversion of lava to talus measured in this study is representative in the longer term, then the total volume of highly pressurized core lava will be less. This may reduce the propensity for hazardous pyroclastic flows derived from a large collapse involving a high proportion of the dome. Also, the implication of being able to measure, via AVTIS data, the volume of lava added to the core over periods of days to weeks is that any variable propensity for hazardous flows could be evaluated in near-real time. As *Calder et al.* [2002] showed, it is during rapid growth of shear lobes, particularly those involving a change in extrusion direction, that collapses are likely to occur over times scales of perhaps a few days. High-frequency measurements by AVTIS would be required to detect this and provide some early warning.

[38] Throughout, we have assumed that the dome growth process measured by AVTIS was entirely exogenous. That is, all the rising magma reached the surface near the summit of the dome and none was added internally to swell the dome or displace the talus [*Hale*, 2008]. There is no reason to doubt this, but AVTIS range change alone is not enough to distinguish between surface deposition and swelling. The uppermost slopes of the dome that expose the core lava and have the highest gradients (>40°), tend not to accumulate new mass and occasionally shed large volumes. Our data were not sufficient to determine whether any differential volume accumulation on different slopes was occurring. During the measurement period there were several departures from the steady state, incremental view of the mass wasting process at the dome as a series of rockfalls (individually unmeasurable by AVTIS), continually transporting mass from the dome summit to the talus. A major loss of mass from the upper eastern part of the dome appears to have occurred on 31 March, during one of the large rockfall events. Downslope from this, mass was accumulating as early as 2 April, particularly after 5 April, and both the Runway and JBH records show deposition increasing to the southeast. A 40-m increase in the elevation of the dome summit appears to occur primarily between 5 and 6 April at the time of a minimum in the number and energy of RF/

LPRF events. This could represent a minor change in the vent extrusion direction as new mass accumulated at the summit. However, despite the reduction in rockfall numbers, the rate of addition to the AVTIS-measurable talus area did not slacken. This may be because these lower energy rockfalls deposited their mass more proximally than at other times.

[39] There is no doubt that AVTIS could yield much more valuable information on the dome growth process with improved temporal and spatial resolution. Rockfalls with typical volumes in the range 10^3–10^4 m^3 occurred about every 15 minutes during our observations. From a closer viewpoint, with improved SNR and faster scan speed it should be feasible to detect the sources and deposits of individual rockfalls. This would enable us, by combining this information with rockfall seismology, to explore the dynamics of the process more fully and to greatly reduce the uncertainties of volume estimation. A continuous audit of the dome core versus talus volumes would also help to evaluate the hazard posed by future large pyroclastic flows involving core lava.

[40] **Acknowledgments.** Dr Vicky Hards is thanked for help with camera data. Helpful reviews by B. Campbell and E. Stofan improved the manuscript. We are grateful to NERC for grant NE/E001734/1 to undertake this work and for their earlier support of the development of AVTIS. GR, SDA, and SCL publish with the permission of the Director, British Geological Survey (NERC).

References

Anderson, S. W., E. R. Stofen, J. J. Plaut, and D. A. Crown (1998), Block size distributions on silicic lava flow surfaces: Implications for emplacement conditions, *Geol. Soc. Amer. Bull.*, *110*, 1258–1267.

Calder, E. S., R. Luckett, R. S. J. Sparks, and B. Voight (2002), Mechanisms of lava dome instability and generation of rockfalls and pyroclastic flows at Soufrière Hills Volcano, Montserrat, in *The Eruption of Soufrière Hills Volcano, Montserrat, From 1995 to 1999, Memoirs*, vol. 21, edited by T. H. Druitt and B. P. Kokelaar, pp. 173–190, Geological Society, London.

Calder, E. S., J. A. Cortes, J. L. Palma, and R. Luckett (2005), Probabilistic analysis of rockfall frequencies during an andesite lava dome eruption: The Soufriere Hills Volcano, Montserrat, *Geophys. Res. Lett.*, *32*, L16309, doi:10.1029/2005GL023594.

Cole, P. D., E. S. Calder, R. S. J. Sparks, A. B. Clarke, T. H. Druitt, S. R. Young, R. A. Herd, C. L. Harford, and G. E. Norton (2002), Deposits from dome-collapse and fountain-collapse pyroclastic flows at Soufrière Hills Volcano, Montserrat, in *The Eruption of Soufrière Hills Volcano, Montserrat, From 1995 to 1999, Memoirs*, vol. 21, edited by T. H. Druitt and B. P. Kokelaar, pp. 231–262, Geological Society, London.

Davies, T. R., M. J. McSavenny, and K. A. Hodgson (1999), A fragmentation-spreading model for long-runout rock avalanches, *Can. Geotech. J.*, *36*, 1096–1110.

Hale, A. J. (2008), Lava dome growth and evolution with an independently deformable talus, *Geophys. J. Int*, *174*, 391–417.

Jolly, A. D., G. Thompson, and G. E. Norton (2002), Locating pyroclastic flows on Soufriere Hills Volcano, Montserrat, West Indies, using amplitude signals from high dynamic range instruments, *J. Volcanol. Geotherm. Res.*, *118*, 299–317.

Jones, L. D. (2006), Monitoring landslides in hazardous terrain using terrestrial LiDAR: An example from Montserrat, *Q. J. Eng. Geol. Hydrogeol.*, *39*, 371–373.

Luckett, R., B. Baptie, and J. Neuberg (2002), The relationship between degassing and rockfall signals at Soufrière Hills Volcano, Montserrat, in *The Eruption of Soufrière Hills Volcano, Montserrat, From 1995 to 1999*, *Memoirs*, vol. 21, edited by T. H. Druitt and B. P. Kokelaar, pp. 595–602, Geological Society, London.

Macfarlane, D. G., and D. A. Robertson (2004), AVTIS—A dual-mode imaging millimetre wave radar/radiometer for volcanological surveying, in *Proceedings of the International Geoscience and Remote Sensing Symposium*, vol. V, pp. 3299–3302, Anchorage, Alaska, Sept. 2004.

Macfarlane, D. G., and D. A. Roberston (2006), A 94 GHz real aperture 3D imaging radar, in *3rd European Radar Conference*, pp. 154–157, Manchester, U.K., Sept. 2006, doi:10.1109/EURAD.2006.280297.

Macfarlane, D. G., G. Wadge, D. A. Robertson, M. R. James, and H. Pinkerton (2006), Use of a portable topographic mapping millimetre wave radar at an active lava flow, *Geophys. Res. Lett.*, *33*, L03301, doi:10.1029/2005GL025005.

Okura, Y., H. Kitahara, T. Sammori, and A. Kawanami (2000), The effects of rockfall volumes on runout distance, *Eng. Geol.*, *58*, 109–124.

Sato, H., T. Fujii, and S. Nakada (1992), Crumbling dacite dome lava and generation of pyroclastic flows at Unzen Volcano, *Nature*, *360*, 664–666.

Sparks, R. S. J., et al. (1998), Magma production and growth of the lava dome of the Soufriere Hills Volcano, Montserrat, West Indies: November 1995 to December 1997, *Geophys. Res. Lett.*, *25*, 3421–3424.

Wadge, G. (2008), Assessing the pyroclastic flow hazards at Soufriere Hills Volcano, Montserrat, in *Advances in Volcanology: The Legacy of G. P. L. Walker*, in press.

Wadge, G., D. G. Macfarlane, D. A. Robertson, A. J. Hale, H. Pinkerton, R. V. Burrell, G. E. Norton, and M. R. James (2005), AVTIS: A novel millimetre-wave ground based instrument for volcano remote sensing, *J. Volcanol. Geotherm. Res.*, *146*, 307–318.

Wadge, G., et al. (2006), Imaging a growing lava dome with a portable radar, *Eos Trans. AGU*, *87/23*, 226–228.

Watts, R. B., R. A. Herd, R. S. J. Sparks, and S. R. Young (2002), Growth patterns and emplacement of the andesitic lava dome at Soufriere Hills, Montserrat, in *The Eruption of Soufrière Hills Volcano, Montserrat, From 1995 to 1999, Memoirs*, vol. 21, edited by T. H. Druitt and B. P. Kokelaar, pp. 115–152, Geological Society, London.

Woods, A. W., R. S. J. Sparks, L. J. Ritchie, J. Batey, C. Gladstone, and M. I. Bursik (2002), The explosive decompression of a pressurized volcanic dome: The 26 December 1997 collapse and explosion of Soufrière Hills Volcano, Montserrat, in *The Eruption of Soufrière Hills Volcano, Montserrat, From 1995 to 1999, Memoirs*, vol. 21, edited by T. H. Druitt and B. P. Kokelaar, pp. 457–465, Geological Society, London.

V. Bass, S. De Angelis, and G. Ryan, Montserrat Volcano Observatory, Flemmings, Montserrat, West Indies.

J. K. Hole, H. M. Odbert, and G. Wadge, Environmental Systems Science Centre, University of Reading, Harry Pitt Building, 3 Earley Gate, Reading, RG6 6AL, UK. (gw@mail.nerc-essc.ac.uk)

M. R. James and H. Pinkerton, Lancaster Environment Centre, Lancaster University, Lancaster, LA1 4YQ, UK.

S. C. Loughlin, British Geological Survey, West Mains Road, Edinburgh, EH9 3LA UK.

D. G. Macfarlane and D. A. Robertson, School of Physics and Astronomy, University of St. Andrews, St. Andrews, KY16 9SS, UK.